Distinct constrictive processes, separated in time and space, divide *Caulobacter* inner and outer membranes

Ellen M. Judd[† 1, 3], Luis R. Comolli[† 4], Joseph C. Chen[3], Kenneth H. Downing[4], W. E. Moerner[2], Harley H. McAdams[* 3]

Departments of Applied Physics[1], Chemistry[2], Stanford University; Developmental Biology[3], Stanford University School of Medicine, Stanford, California 94305; Life Sciences Division[4], Lawrence Berkeley National Laboratory, Berkeley, California 94720

[†]equal contributions.

Running title: Distinct constrictive processes

*Corresponding Author:

Harley H McAdams

Department of Developmental Biology

Stanford University School of Medicine

279 Campus Drive, Beckman Center B300

Stanford, CA 94305-5329

hmcadams@stanford.edu

Phone: (650) 858-1864

FAX: (650) 725-7739

ABSTRACT

Cryo-electron microscope tomography (cryoEM) and a fluorescence loss in photobleaching (FLIP) assay were used to characterize progression of the terminal stages of *Caulobacter crescentus* cell division. Tomographic cryoEM images of the cell division site show separate constrictive processes closing first the inner, and then the outer, membrane in a manner distinctly different from septum-forming bacteria. The smallest observed pre-fission constrictions were 60 nm for both the inner and outer membrane. FLIP experiments had previously shown cytoplasmic compartmentalization, when cytoplasmic proteins can no longer diffuse between the two nascent progeny cell compartments, occurring 18 min before daughter cell separation in a 135 min cell cycle. Here, we used FLIP experiments with membrane-bound and periplasmic fluorescent proteins to show that (i) periplasmic compartmentalization occurs after cytoplasmic compartmentalization, consistent with the cryoEM observations, and (ii) inner membrane and periplasmic proteins can diffuse past the FtsZ constriction site, indicating that the cell division machinery does not block membrane diffusion.

INTRODUCTION

The early stages of bacterial cytokinesis, involving septal ring assembly and constriction, are better understood than the terminal stages. In this work we investigate the late stages of cytokinesis in the gram negative bacterium *Caulobacter crescentus*. We use fluorescence loss in photobleaching (FLIP) and cryo-electron microscope tomography (cryoEM) to determine (i) the geometry of the inner and outer membranes at various stages of cell division, (ii) the timing of inner membrane and periplasm compartmentalization and, (iii) whether the FtsZ ring and associated cell division machinery hinders diffusion of membrane-bound or periplasmic molecules through the division plane in predivisional cells.

Caulobacter crescentus divides asymmetrically, producing two distinct daughter cells: the swarmer cell and the stalked cell (Fig. 1). These cells differ in their transcription programs, protein composition, and behavior (3, 22, 28, 32). The daughter cells also differ in size; the nascent swarmer cell compartment is about 2/3 as long as the nascent stalked cell compartment. After cell division, swarmer cells undergo an initial motile phase, and then they differentiate into stalked cells; they lose their flagellum and pili, and DNA replication is initiated. The compartmentalization of the predivisional cell is an important step in the process of creating daughter cells with different cell fates. Immediately after cytoplasmic compartmentalization, the complement of cytoplasmic proteins in the two compartments can begin to diverge, launching the two daughter cells on different developmental paths. The physical compartmentalization of the *Caulobacter* cytoplasm well before cell division triggers a phosphotransport-based switch mechanism

that initiates the differential regulation of development in the nascent daughter cells (21, 23).

Many proteins involved in cytokinesis are known in *Escherichia coli* and *Bacillus subtilis* (1, 19, 35) and to a lesser extent in *Caulobacter crescentus* (19, 20, 26, 27, 29). In each of these species, the widely-conserved tubulin-like FtsZ protein initiates cell division by polymerizing into a ring at the future division site. After initial formation of the ring, additional protein components of the division apparatus are recruited into the ring at various times during progression to cell division. This large FtsZ-based protein complex is called the septal ring. The details of the function and protein composition of the septal ring in late stages of bacterial cytokinesis are both less understood than earlier stages and more variable across different species (13). In *Caulobacter*, the FtsZ ring forms at the division plane about 90 min into a 180 min cell cycle; about 30 min later, constriction of the cell is visible by light microscopy. From first visible constriction to cell separation takes about 60 min (27).

Conceptual models of the FtsZ ring depict the ring located close to the inner side of the inner membrane and attached to the inner membrane in some manner to effect the inward-directed force that constricts the cell at the division plane [for example, see Figure 2 of Addinal, 2002 (1)] In *E. coli*, both FtsA and ZipA function to tether FtsZ to the inner membrane (25). In mutant *E. coli* strains that form a short partial spiral, rather than a circumferential ring, of FtsZ, sharp indentation in the cell envelope is observed along the spiral arc in scanning EM images (2). This observation shows that the constrictive force is a local phenomenon along segments of the FtsZ ring, rather than being the consequence of constriction by a "purse string" structure. So, although details of the

physical association of the ring and the inner membrane are unknown, the connection is sufficiently strong and continuous in *E. coli* cells that the ring can pull the cell envelope sharply inward along the length of the ring. The *E. coli* FtsZ proteins are located at the leading edge of the septal invagination (4). One can easily imagine that the FtsZ ring might be a physical obstacle to diffusion for membrane-bound proteins, effectively partitioning the inner membrane surface into two compartments after formation of the ring. This possibility motivated our FLIP assay to measure the diffusion of fluorescent-tagged membrane-bound proteins through the division plane.

A FLIP assay was previously used to show that the *Caulobacter crescentus* cytoplasm is compartmentalized about 18 min before cell separation in a 135 minute cell cycle (16). Here, we report the use of a similar FLIP assay with fluorescently tagged membrane-bound and periplasmic proteins to examine the terminal stages of *Caulobacter* cytokinesis. We show that the periplasm becomes compartmentalized after the cytoplasm, and we observe membrane-bound and periplasmic proteins diffusing past the septal ring. We also used high resolution (~60 Å) cryoEM tomography to image *Caulobacter* cells at successive stages of cell division. These images show that the late stages of constriction and fission of the *Caulobacter* inner and outer membrane are distinct events occurring one after the other, and distinctively separated in time and space, consistent with the FLIP assay results.

MATERIALS AND METHODS

Bacterial strains and plasmids. Strain LS4026 is strain PV2398 with the plasmid pEJ178. PV2398 is strain CB15N, with the *pilA* gene fused to the N-terminal of EGFP

under the control of the *pilA* promoter, integrated into the chromosome at the *pilA* locus (Patrick Viollier, unpublished). Plasmid pEJ178 is pJS14 based, and contains the *tdimer2* gene (8) under the control of the xylose promoter, with the xylose promoter in the same orientation as the lac promoter.

Strain LS4029 is strain CB15N, with plasmids pEJ178 and pEJ204. Plasmid pEJ204 is pMR10 based and contains the CC2909 gene fused to EGFP under the control of the xylose promoter, with the xylose promoter in the opposite orientation from the lac promoter. CC2909 is a histidine kinase of unknown function with 2 predicted transmembrane domains.

Strain LS4032 is strain LS3008 with the plasmid pEJ216. LS3008 is strain CB15N, with the EGFP gene under the control of the xylose promoter, integrated into the chromosome at the xylose locus. Plasmid pEJ216 is pJS14 based, with the signal sequence of *torA* (9, 30, 34) from *E. coli* fused to the N-terminal of the *tdimer2* gene, under the control of the xylose promoter, with the xylose promoter in the same orientation as the lac promoter.

Strain LS2677, used as a control in the fractionation experiments, is CB15N with the pJS14 plasmid.

Bacterial growth media. *Caulobacter crescentus* strains were grown in PYE complex media (12) or M2G minimal media at 28° C. M2G was made as previously described, (12) but using 8.7 g/l Na_2HPO_4, 5.3 g/l KH_2PO_4, 0.2% glucose, and 0.5 mM $MgSO_4$ in place of 0.5 mM $MgCl_2$. Media were supplemented with kanamycin (5 μg/ml) or chloramphenicol (1 μg/ml) as necessary. Transcription from the xylose promoter was induced by adding 0.3% xylose to the growth media. Cells were grown overnight in

PYE. They were then washed and diluted in M2G, and incubated until the A_{660} reached ~0.2. Cells were then diluted to an A_{660} of ~ 0.05 in M2GX (M2G + 0.3% xylose) to induce transcription from the xylose promoter. Strain LS4032 was induced for 3-6 hours prior to imaging. Strains LS4026 and LS4029 were induced for at least 8 hours prior to imaging. During induction, cultures were diluted as necessary to keep the $A_{660} < 0.2$.

An aliquot of these cells was harvested and spread on a pad of 1% agarose (Sigma, A-0169) in M2GX media, mounted on a 25 mm x 75 mm glass slide. The slide was sealed with valap (1:1:1 vaseline:lanolin:paraffin). The cells grew and divided on the slides, and data collection lasted no more than 1 hour on each slide.

Cell fractionation. Separation of *C. crescentus* cell lysates into soluble and membrane fractions was performed as previously described (9), except cells were grown until A600 reached 0.3-0.4, and incubation with lysozyme lasted for 5 min at room temperature and 5 min on ice.

Periplasmic proteins were isolated using the same spheroplast formation method as previously described (31), except that ethylenediamine tetraacetic acid (EDTA) and lysozyme were added to final concentrations of 1 mM and 10 μg/ml, respectively.

Fluorescence microscopy and photobleaching. Fluorescence microscopy was performed on a Nikon Diaphot 200 inverted microscope with a Nikon PlanApo 100X objective with a numerical aperture of 1.4. Images were recorded with a Princeton Instruments MicroMax CCD camera (NTE/CCD-512-EBFT.GR-1). A Novalux Protera frequency-doubled semiconductor laser with a wavelength of 488 nm was used for illumination. A lens of focal length 30 cm (Newport, KPX112 AR.14) was placed 30 cm

from the back focal plane of the microscope objective, on a mount that allowed the lens to be moved in and out of the beam path. With the lens in the path, the laser formed a Gaussian spot with a full-width-half-maximum (FWHM) size of 9 μm. Without the lens, the FWHM size was 0.4 μm. The compartmentalization assay was performed as follows: a cell, immobilized on an agarose pad, was positioned with one end at the focal point of the laser. The cell was imaged in wide field mode with the lens in the beam path. The lens was removed from the path and the cell was bleached with the focused beam. The lens was put back into the beam and the cell was imaged again. The exposure time for each wide field image was 1 second.

To image both the tdimer2 and the EGFP signals simultaneously, we used two Q570LP dichroics (Chroma Technology Corp) to separate the two colors and direct them to different regions of the CCD. To reduce crosstalk we used a HQ525/50M bandpass filter (Chroma) (strains LS4026, LS4029, LS4032) or a 535DF55 bandpass filter (Omega Optical Inc) (strain LS4032) filter in the EGFP beam path and a E580LPM filter (Chroma) in the tdimer2 beam path. The dichroic in the microscope (to separate the excitation and emission light) was a Q495LP (Chroma).

For experiments on strain LS4026, the laser power was 100 μW entering the microscope. The laser was attenuated using a neutral density filter with an optical density (OD) of 1 during the bleaching pulse. The bleaching pulse was 30 s long, followed by a 20 s pause before the second image was taken.

For experiments on strain LS4029, the laser power was 200 μW entering the microscope. The laser was attenuated using a neutral density filter with an OD of 1.5 during the

bleaching pulse. The bleaching pulse was 240 s long, followed by a pause of approximately 20 s, while the microscope was refocused, before the second image was taken.

For experiments on strain LS4032, the laser power was 200 μW entering the microscope. The laser was attenuated using a neutral density filter with an optical density (OD) of 1 during the bleaching pulse. The bleaching pulse was 5 s long, followed by a 2 s pause before the second image was taken.

Fluorescence image analysis. Image analysis was performed as previously described, using the Matlab Image Processing Toolbox (16). For compartmentalization assay images, the average fluorescence intensity in the cell compartment distal to the focused laser spot was computed before and after the bleaching pulse for both the red and the green channels. The percent changes in average intensity (ΔI_{d_red}, ΔI_{d_green}) were calculated. Images from the control experiment, in which the bleaching laser was focused outside of the cell, were analyzed by computing the average intensity of the whole cell before and after "bleaching" (ΔI_{red}, ΔI_{green}). The percent decrease in fluorescence intensity of these control cells after the "bleaching" pulse was calculated. The decrease in fluorescence signal in these control cells is due to nonspecific bleaching by the tails of the laser spot and by the wide field illumination used for imaging.

For strain LS4026 ΔI_{red} ranged from 8% to 54% and ΔI_{green} ranged from 2% to 39%. LS4026 cells for which $\Delta I_{d\_red} < 55\%$ were said to have a compartmentalized cytoplasm. If $\Delta I_{d\_red} > 55\%$ the cytoplasm was deemed not compartmentalized. Cells for which

$\Delta I_{d\_green} < 40\%$ were said to have a compartmentalized inner membrane. If $\Delta I_{d\_green} > 40\%$ the inner membrane was deemed not compartmentalized.

For strain LS4032 ΔI_{red} ranged from 13% to 43% and ΔI_{green} ranged from 4% to 42%. LS4032 cells for which $\Delta I_{d\_red} < 50\%$ were said to have a compartmentalized periplasm. If $\Delta I_{d\_red} > 50\%$ the periplasm was not compartmentalized. Cells for which $\Delta I_{d\_green} < 50\%$ were said to have a compartmentalized cytoplasm. If $\Delta I_{d\_green} > 50\%$ the cytoplasm was not compartmentalized.

Cryo-electron microscopy. *Caulobacter crescentus* cells were grown in liquid PYE media at 30 degrees C for six to eight hours until reaching an A_{610} between 0.4 and 0.7. Cells were synchronized as described previously (14) and resuspended in M2G to a final A_{610} between 0.4 and 0.5.. The synchronized cells were grown for 120 min at 30 degrees. The cell cycle was approximately 135 minutes long under these growth conditions. Aliquots of 5 μl were then taken directly from the culture and placed onto glow discharged lacey carbon grids (Ted Pella 01881). The grids were manually blotted and plunged into liquid ethane, then stored in liquid nitrogen.

All images were acquired in a JEOL-3100-FEF electron microscope with a Field Emission Gun (FEG) electron source operating at 300 kV. The instrument was equipped with an energy filter, a 2k by 2k CCD camera (Gatan 795), and a cryo transfer stage. Cells were imaged at 80 deg K (using liquid nitrogen) and 16 degrees K (using liquid He).

Tomographic tilt series were acquired under low dose conditions, typically over an angular range between +65 deg and -65 deg, ± 5 deg with increments of 1.5 deg or 2 deg. Between 70 and 90 images were recorded for each series. All data sets were acquired using DigitalMicrograph (Gatan).

All images were recorded using a magnification of 32 K (nominal value 25K with 1.4X post-column magnification) giving a pixel size of 1 nm at the specimen, underfocus of 6.4 μm ± 0.5 um, and energy filter widths of 32 ev to 50 ev. The maximum dose used per complete tilt series was 80 electrons per $Å^2$ (e-/$Å^2$), with typical values of approximately 70 e-/$Å^2$. A total of 10 tomographic reconstructions was acquired.

A series of two-dimensional projections of *Caulobacter* cells at different stages of the cell division cycle were also acquired using doses between 16 e-/$Å^2$ and 50 e-/$Å^2$ per image. A total of about 200 cells was imaged.

The IMOD package (17) was used for image processing and tomographic reconstructions by backprojection. The program ImageJ (NIH, http://rsb.info.nih.gov/ij/) was used for analysis of the two-dimensional image projections. Volume rendering, surface rendering and image analysis used the packages AVS Express (AVS Advanced Visual Systems, http://www.avs.com/index_wf.html) and VolView (KitWare).

RESULTS

Electron microscope images of the dividing cell. To characterize the end stages of *Caulobacter* cytokinesis, images of whole *Caulobacter* cells were collected in three

dimensions using cryoEM tomography. Figure 2 shows a series of cryoEM images at successive stages of *Caulobacter* cell division. Panels A and B are slices from 3D tomographic images. Panels C-E are 2D transmission cryoEM images. Initial stages of *Caulobacter* cell constriction involve an extended pinching of the cell (Fig. 2A). The distance between the inner and outer membranes is constant at approximately 30 nm throughout the cell. Even in the higher quality source images, we are unable to reliably identify the murein sacculus layer, so we were not able to determine how it associates with either the inner or outer membrane as constriction progresses. In later stages of division (Figs. 2B, 3A), constriction of the inner membrane proceeds ahead of outer membrane constriction, and the inter-membrane spacing at the constriction site widens from the constant spacing seen elsewhere. This may involve dissolution of intermembrane structural components to enable separation of the membranes. The constriction of the inner membrane continues until the inner membranes of the two nascent cell compartments are connected only by a small tubular section (Figs. 2B, 3A). This small passage connecting the two cytoplasmic compartments would not be visible without the three dimensional cryoEM tomographic data. Figure 3A shows a volume-rendered view of this same cell with the inner and outer membranes segmented for clarity. A dynamic three-dimensional view of this stage of the cell is available in the supplemental material at http://caulo.stanford.edu/usr/hm/media/caulob3D.mpg. Next, the inner membrane parts, and the cytoplasm is separated into two compartments (Fig. 2C), while the outer membrane remains continuous. After fission of the inner membrane, constriction of the outer membrane continues (Figs. 2C,D) until there is again only a small section connecting the two daughter cells. We captured only one cell in this very

late stage. Because we don't have 3D tomographic data for this cell, we don't know if the periplasm of the daughter cells is still connected through the middle of the remaining outer membrane tubular structure seen in Figure 2D. Except in the immediate vicinity of this connecting section, the inner membrane-outer membrane spacing is once again "normal", i.e. approximately 30 nm over the entire cell surface. Finally, the outer membrane parts, and cytokinesis is complete (Fig. 2E).

To characterize the physical properties of membrane fission, we measured the smallest observed constriction width and radius of curvature of the inner and outer membranes (Fig. 2F). The smallest inner membrane connection we observed (Fig. 2B) was 60 nm in diameter and the radii of curvature of the inner membrane at the constriction were 20 nm and 25 nm (two values in the same cell because the cell was slightly bent). The radius of curvature of the inner membrane at the cell pole after fission (Fig. 2C) was approximately 90 nm. The smallest outer membrane connection we observed (Fig. 2D) was 60 nm in diameter and the radii of curvature of the outer membrane at the constriction were 22 nm and 16 nm.

The cytoplasm is compartmentalized before the periplasm. To compare the timing of the compartmentalization of the cytoplasm and the periplasm, we used the FLIP compartmentalization assay on strain LS4032, expressing both cytoplasmic EGFP and periplasmic tdimer2. tdimer2 was fused to the signal sequence of the *E. coli* TorA protein (ssTorA) to cause it to be exported to the periplasm. Western blots of fractionated cells (Fig. 4A) show that ssTorA-tdimer2 is in the *Caulobacter* periplasm and that soluble EGFP remains in the spheroplast fraction. We performed immunoblot analysis on spheroplast and periplasmic fractions from LS4032 cells (Fig. 4A). Probing

with anti-GFP antibody revealed that EGFP was in the spheroplast fraction, while probing with anti-tdimer2 antibody showed that tdimer2 was in the periplasmic fraction.

For the FLIP compartmentalization assay (16), the red (ssTorA-tdimer2) and green (EGFP) fluorescence signals were imaged in single cells. The cells were then bleached with a laser focused at one end of the cell (Fig. 5, left panels), and a second fluorescence image was taken of the bleached cells (Fig. 5, center panels). Cells that appeared compartmentalized in the second image were imaged again 10 min after bleaching (Figs. 5B, C, D, right panels). We refer to the end of the cell that received the laser pulse as the proximal end, and the other end of the cell as the distal end. In a cell that is not compartmentalized, proteins initially located throughout the cell will diffuse through the focused laser beam during the bleaching pulse and be photobleached. This cell will appear dark in the second fluorescence image, since all the fluorescent proteins in the cell have then been bleached. In a compartmentalized cell, proteins in the distal portion of the cell cannot diffuse into the proximal portion of the cell, and therefore do not get bleached by the focused laser. In the compartmentalized cell, the distal portion of the cell will remain fluorescent in the second fluorescence image. Some decrease in fluorescence signal will occur in all cells due to nonspecific bleaching by the tails of the laser spot and by the wide field illumination used for imaging.

By performing this FLIP assay on cells in which the cytoplasm and the periplasm were labeled with differently colored fluorescent proteins, we determined the compartmentalization state of both the periplasm and the cytoplasm in individual cells. LS4032 cells were bleached for 5 s, and the second image was taken 2 s after the end of the bleaching pulse. After bleaching, a cell in which the cytoplasm is not yet

compartmentalized will display no EGFP fluorescence signal, and a cell in which the periplasm is not yet compartmentalized will display no tdimer2 signal. A cell in which the cytoplasm is compartmentalized will retain an EGFP signal in the distal compartment, and a cell in which the periplasm is compartmentalized will retain a tdimer2 signal in the distal compartment. We performed this two-color assay on late predivisional cells (selected from a mixed population by morphology). Of the 40 LS4032 cells treated with the FLIP assay, 24 had neither the cytoplasm nor the periplasm compartmentalized (Fig. 5A), while 12 cells had compartmentalized cytoplasm and periplasm (Fig. 5B). In three cells, both the cytoplasm and the periplasm appeared compartmentalized 2 s after bleaching, but the red fluorescence signal had spread to the proximal part of the cell in the third image, taken after 10 min, indicating that the periplasm was not fully compartmentalized (Fig. 5C). One cell had red fluorescence, but not green fluorescence, remaining in the distal portion of the cell 2 s after bleaching. However, when this cell was imaged again after 10 min, red fluorescence signal was again present in the proximal part of the cell (Fig. 5D), indicating that slow periplasmic diffusion was still occurring between the two cell compartments, and that the periplasm was not fully compartmentalized. Therefore we conclude that of the 49 cells assayed, at least 3 had compartmentalized cytoplasm but not compartmentalized periplasm, indicating that the cytoplasm becomes compartmentalized before the periplasm. Also, it appears that at some time prior to compartmentalization of the periplasm, diffusion in the periplasm through the cell division site is dramatically slowed.

We observed diffusion of a periplasmic protein past the constriction site of predivisional cells (Figs. 5A, C, D). The FtsZ ring and associated cell division machinery are present

at the division site prior to constriction. Therefore we conclude that the septal ring does not block diffusion of periplasmic proteins, though it may obstruct their passage somewhat as the cell nears separation, causing the slow intercompartmental diffusion seen in some cells.

The septal ring does not block diffusion in the inner membrane. To compare the timing of the compartmentalization of the cytoplasm and the inner membrane and to determine if the septal ring blocks diffusion of inner membrane proteins, we performed a FLIP compartmentalization assay similar to the one described above on two strains, LS4026 and LS4029, each containing cytoplasmic tdimer2 (8) and EGFP fused to an inner membrane-bound protein. Strain LS4026 contains cytoplasmic tdimer2 and membrane-bound pilA-EGFP. PilA is a pilus subunit that is predicted to have a single transmembrane domain (33). Strain LS4029 contains cytoplasmic tdimer2 and membrane-bound CC2909-EGFP. CC2909 is a histidine kinase of unknown function with 2 predicted transmembrane domains. Western blots of fractionated cells (Fig. 4B) show that both PilA-EGFP and CC2909-EGFP were found in the membrane fraction and that tdimer2 remains in the cytoplasm of *Caulobacter* cells. We performed immunoblot analysis on soluble and periplasmic fractions from LS4026 and LS4029 cells (Fig. 4A). Probing with anti-GFP antibody revealed that PilA-GFP and CC2909-GFP were in the membrane fraction, while probing with anti-tdimer2 antibody showed that tdimer2 was in the soluble fraction.

All of the 50 LS4026 cells observed with the FLIP assay had either both the cytoplasm and inner membrane compartmentalized, or neither the cytoplasm nor the inner membrane compartmentalized (images not shown). This result suggests that the inner

membrane and the cytoplasm become compartmentalized at the same time. 28 of the 30 LS4029 cells had either both the cytoplasm and inner membrane compartmentalized, or neither the cytoplasm nor the inner membrane compartmentalized. However, two of the LS4029 cells had the inner membrane compartmentalized but not the cytoplasm (images not shown). This result suggests that the inner membrane could be compartmentalized before the cytoplasm. It is possible that the compartmentalization time is different for the two proteins. There may be a barrier related to the constriction apparatus that forms shortly before the compartmentalization of the cytoplasm that prevents diffusion of CC2909-EGFP (an 88 kDa protein) past the division site, but allows passage of PilA-EGFP (a 33 kDa protein). It also possible that these results arise from the differences in the physical geometry of the dividing cells combined with the much slower diffusion in the membrane compared to the cytoplasm. The cryoEM images described above show that at one point in the division process, cells have a highly constricted, but not completely closed, inner membrane. In the two LS4029 cells in which the membrane appeared to be compartmentalized but not the cytoplasm, it may be that the membrane was not fully compartmentalized, but that diffusion in the membrane past the division site was slowed due to the constriction of the membrane. If the diffusion past the division site was slowed enough, the membrane would appear compartmentalized in our assay. This slowing of diffusion would be more noticeable in strain LS4029 than in strain LS4026 because CC2909-EGFP diffuses more slowly than PilA-EGFP.

In both strains LS4026 and LS4029 we observed diffusion of inner membrane proteins past the constriction site in the majority of predivisional cells (Figs. 6A, B). The septal ring is present at the division site prior to the start of constriction, so we conclude that the

septal ring alone does not block diffusion of inner membrane proteins. However, six of the LS4029 cells assayed showed green fluorescence, but no red fluorescence, in the distal half of the cell 20 s after bleaching, but when imaged again 10 min after bleaching, the remaining green fluorescence had spread from the distal half of the cell into the proximal half (Fig. 6B). We cannot determine the precise stage of cell constriction with the light microscope, but some small fraction of the cells in the observed sample would be nearing inner membrane separation. We interpret the observation of a few cells showing slow diffusion of inner membrane-bound proteins across the constriction site as evidence that diffusion is slowed near the time of cell division, consistent with the cryoEM images that show a highly constricted inner membrane (Figs. 2B, 3A).

DISCUSSION

Our cryoEM images of the dividing *Caulobacter* cells show that in early stages of cell division, the inner and outer membranes constrict simultaneously, maintaining the 30 nm separation seen in regions distant from the constriction. As cell division progresses, the inner and outer membranes separate near the constriction site, and fission of the inner membrane occurs before fission of the outer membrane, leading to a cell that contains two inner membrane-bound cytoplasmic compartments surrounded by a single continuous outer membrane. These images show that distinct processes control inner and outer membrane constriction in the later stages of cell division. Early constriction of the inner membrane is effected by the FtsZ ring and associated proteins (13, 35). Separate protein structures controlling late constriction of the outer membrane have not yet been identified.

The constriction in each membrane becomes remarkably small (less than 60 nm in diameter) before unknown terminal events effect complete closure. These highly constricted membranes are also tightly bent, with a radius of curvature of 20 nm or less. The bent membrane (inner membrane in Fig. 2B) may break spontaneously, and then reseal around the cytoplasm of the nascent daughter cell, with a significantly larger radius of curvature (inner membranes in Fig. 2C). In other words, the final fission event may occur simply because the two surface configuration is a lower energy state for the lipid membrane structure. After inner and outer membrane fission we did not observed any evidence for a residual "scar" in either membrane (Figs. 2C, 2E).

The use of the tomographic cryoEM technique to generate a three dimensional image of the cell allowed us to observe a very small channel connecting the cytoplasm of a predivisional cell prior to cytoplasmic compartmentalization (Figs. 2B, 3A). Channels of this size are not visible in 2D images of whole cells. When cells are sliced before imaging, it is extremely unlikely to slice a cell exactly down the middle, and therefore the small connecting hole would easily be missed.

The cryoEM tomographic images are consistent with the FLIP experiments used to characterize the diffusion of proteins past the constriction site. We reported previously that the cytoplasm of *Caulobacter* cells becomes compartmentalized (so that cytoplasmic proteins can no longer diffuse between the nascent progeny cells) about 18 min prior to daughter cell separation (16). Here we show that the periplasm is compartmentalized later than the cytoplasm. These results are consistent with the EM images in which the inner membrane is sealed between the cytoplasms of the two daughter cells, but the periplasmic space remains continuous (Figs. 2C, 3B).

The FLIP experiments show that both inner membrane and periplasmic proteins are able to diffuse past the site of constriction. The FtsZ ring and associated proteins (called the septal ring) form a ring-like structure attached to the inner membrane at the constriction site (13, 35). The mode of attachment to the membrane is unknown. It is also unknown whether the septal ring is a continuous ring. It is possible that the septal ring is continuous, but only attached to the inner membrane at discrete points. Alternatively, there may be breaks in the ring that allow membrane proteins to diffuse through. FtsZ is known to turn over rapidly, which may cause transient breaks in the ring. The slow diffusion of membrane and periplasmic proteins through the division site observed for some cells could be due to the very small dimension of the remaining connection as the compartments near separation (Figs. 2B, 2D, 2F). Or, the constriction machinery may congest the connection as the constriction nears separation.

The measured diffusion coefficient for the inner membrane protein PleC-EYFP is D = (12 ± 2) $x10^{-3}$ $\mu m^2/s$ (10). This is roughly 200 times smaller than the D value of (2500 ± 600) $x10^{-3}$ $\mu m^2/s$ measured by fluorescence recovery after photobleaching for a cytoplasmic protein of similar mass (GFP fused to a maltose-binding protein domain, 72 kDa) in *E. coli* (11). Our results reported here for the FLIP experiments are consistent with slower diffusion of proteins in the inner membrane than in the cytoplasm. All the cytoplasmic EGFP in a cell could be bleached with a laser focused at one end of the cell for 5 s (10). The membrane-bound EGFP, however, required localized bleaching for from 30 s (for PilA-EGFP) to 240 s (for CC2909-EGFP) to completely bleach the cell independent of the laser intensity. This indicates that the membrane-bound EGFP fusion proteins took longer to diffuse from the far end of the cell into the laser beam than did the

cytoplasmic EGFP. If this difference in diffusion coefficient between membrane-bound and cytoplasmic proteins holds for a large number of proteins, it could have interesting implications for cellular structure and the regulation of cellular asymmetry. The small D of membrane-bound proteins would make it easier for cells to maintain a non-uniform distribution of these proteins, such as a gradient of protein concentration across the length of the cell. Such non-uniform concentrations could be utilized to regulate cellular asymmetry. Cytoplasmic proteins, on the other hand, would be better suited to rapidly carrying signals from one part of the cell to another. The difference in diffusion coefficient between membrane-associated and cytoplasmic proteins has been shown to be important for the proper functioning of the oscillation of the MinCDE proteins in *E. coli* (15, 18, 24).

Electron microscope images show that in *E. coli* and *B. subtilis*, the inner membrane and the cell wall invaginate together, forming a septum, and the outer membrane constricts later (5-7). Figure 3B shows the progression of *Caulobacter* cell division schematically based on the images in Figure 2 with an approximately consistent scale. For comparison, Figure 3C shows a schematic of progression of *E. coli* cell division (adapted with permission from Figure 32 in Burdett and Murray, 1974) (6). The differences with the *Caulobacter* cell division process are striking. Our images of *Caulobacter* division do not have the exterior blebs and interior mesosomes seen in the *E. coli* images, but these could be artifacts of the fixation and slicing procedures involved at the time in producing the EM images on which the diagram in Figure 3C is based. In *E. coli* inner membrane constriction also precedes outer membrane constriction, but the constriction of the inner membrane involves physical association of the two inner membranes of the nascent

daughter cells to form the septal disk. Later, after closure of the septum, the *E. coli* outer membrane constricts between the two inner membrane surfaces and separates the cell. In other EM images of *E. Coli*, it appears that the inner and outer membranes invaginate together (4). We have not found published cryoEM images of the *E. coli* and *B. subtilis* cytokinesis. When such images become available, it will be possible to make a more direct comparison of the cell division processes in *Caulobacter* and in the septum-forming bacteria. The geometric differences in the cell constriction and separation process between *Caulobacter*, *E. coli*, and *B. subtilis* suggest there are striking differences between the *Caulobacter* terminal cell constriction and closure mechanisms compared to the septum-forming bacteria. The spatial separation of the *Caulobacter* inner and outer membrane constrictive rings will facilitate labeling and identification of the proteins in the separate structures.

ACKNOWLEDGEMENTS

EMJ and HHM were supported by Office of Naval Research grant N00014-02-1-053. The Director, Office of Science, Office of Basic Energy Sciences, of the U.S. Department of Energy provided support under Contract No. DE-AC03-76SF00098 (LRC and KD), grant DE-FG03-01ER63219-A001 (HHM), and grant DE-FG02-04ER63777 (WEM). JCC was supported by National Institutes of Health grant F32 G067472.

VolView was used under a personal free license from KitWare. The movies and isosurfaces shown in Supplementary Materials were done in collaboration with the Scientific Visualization Group at LBNL. We thank Patrick Viollier (Case Western University) for providing the PilA-GFP strain.

REFERENCES

1. **Addinall, S. G., and B. Holland.** 2002. The tubulin ancestor, FtsZ, draughtsman, designer and driving force for bacterial cytokinesis. J Mol Biol **318:**219-36.

2. **Addinall, S. G., and J. Lutkenhaus.** 1996. FtsZ-spirals and -arcs determine the shape of the invaginating septa in some mutants of *Escherichia coli*. Mol Microbiol **22:**231-7.

3. **Ausmees, N., and C. Jacobs-Wagner.** 2003. Spatial and temporal control of differentiation and cell cycle progression in *Caulobacter crescentus*. Annu Rev Microbiol **57:**225-47.

4. **Bi, E. F., and J. Lutkenhaus.** 1991. FtsZ ring structure associated with division in *Escherichia coli*. Nature **354:**161-4.

5. **Burdett, I. D.** 1979. Electron microscope study of the rod-to-coccus shape change in a temperature-sensitive rod- mutant of *Bacillus subtilis*. J Bacteriol **137:**1395-405.

6. **Burdett, I. D., and R. G. Murray.** 1974. Electron microscope study of septum formation in *Escherichia coli* strains B and B-r during synchronous growth. J Bacteriol **119:**1039-56.

7. **Burdett, I. D., and R. G. Murray.** 1974. Septum formation in *Escherichia coli*: characterization of septal structure and the effects of antibiotics on cell division. J Bacteriol **119:**303-24.

8. **Campbell, R. E., O. Tour, A. E. Palmer, P. A. Steinbach, G. S. Baird, D. A. Zacharias, and R. Y. Tsien.** 2002. A monomeric red fluorescent protein. Proc Natl Acad Sci U S A **99:**7877-82.

9. **Chen, J. C., P. H. Viollier, and L. Shapiro.** 2005. A membrane metalloprotease participates in the sequential degradation of a *Caulobacter* polarity determinant. Mol Microbiol **55:**1085-103.

10. **Deich, J., E. M. Judd, H. H. McAdams, and W. E. Moerner.** 2004. Visualization of the movement of single histidine kinase molecules in live *Caulobacter* cells. Proc Natl Acad Sci U S A **101:**15921-6.

11. **Elowitz, M. B., M. G. Surette, P. E. Wolf, J. B. Stock, and S. Leibler.** 1999. Protein mobility in the cytoplasm of *Escherichia coli*. J Bacteriol **181:**197-203.

12. **Ely, B.** 1991. Genetics of *Caulobacter crescentus*. Methods Enzymol **204:**372-84.

13. **Errington, J., R. A. Daniel, and D. J. Scheffers.** 2003. Cytokinesis in bacteria. Microbiol Mol Biol Rev **67:**52-65.

14. **Evinger, M., and N. Agabian.** 1977. Envelope-associated nucleoid from *Caulobacter crescentus* stalked and swarmer cells. J Bacteriol **132:**294-301.

15. **Howard, M., A. D. Rutenberg, and S. de Vet.** 2001. Dynamic compartmentalization of bacteria: accurate division in *E. coli*. Phys Rev Lett **87:**278102.

16. **Judd, E. M., K. R. Ryan, W. E. Moerner, L. Shapiro, and H. H. McAdams.** 2003. Fluorescence bleaching reveals asymmetric compartment formation prior to cell division in *Caulobacter*. Proc Natl Acad Sci U S A **100:**8235-40.

17. **Kremer, J. R., D. N. Mastronarde, and J. R. McIntosh.** 1996. Computer visualization of three-dimensional image data using IMOD. J Struct Biol **116:**71-6.

18. **Kruse, K.** 2002. A dynamic model for determining the middle of *Escherichia coli*. Biophys J **82:**618-27.

19. **Margolin, W.** 2003. Bacterial division: the fellowship of the ring. Curr Biol **13:**R16-8.

20. **Martin, M. E., M. J. Trimble, and Y. V. Brun.** 2004. Cell cycle-dependent abundance, stability and localization of FtsA and FtsQ in *Caulobacter crescentus.* Mol Microbiol **54:**60-74.

21. **Matroule, J. Y., H. Lam, D. T. Burnette, and C. Jacobs-Wagner.** 2004. Cytokinesis monitoring during development; rapid pole-to-pole shuttling of a signaling protein by localized kinase and phosphatase in *Caulobacter*. Cell **118:**579-90.

22. **McAdams, H. H., and L. Shapiro.** 2003. A bacterial cell-cycle regulatory network operating in time and space. Science **301:**1874-7.

23. **McGrath, P. T., P. Viollier, and H. H. McAdams.** 2004. Setting the pace: mechanisms tying Caulobacter cell-cycle progression to macroscopic cellular events. Curr Opin Microbiol **7:**192-7.

24. **Meinhardt, H., and P. A. de Boer.** 2001. Pattern formation in *Escherichia coli*: a model for the pole-to-pole oscillations of Min proteins and the localization of the division site. Proc Natl Acad Sci U S A **98:**14202-7.

25. **Pichoff, S., and J. Lutkenhaus.** 2005. Tethering the Z ring to the membrane through a conserved membrane targeting sequence in FtsA. Mol Microbiol **55:**1722-34.

26. **Quardokus, E. M., and Y. V. Brun.** 2002. DNA replication initiation is required for mid-cell positioning of FtsZ rings in *Caulobacter crescentus*. Mol Microbiol **45:**605-16.

27. **Quardokus, E. M., N. Din, and Y. V. Brun.** 2001. Cell cycle and positional constraints on FtsZ localization and the initiation of cell division in *Caulobacter crescentus*. Mol Microbiol **39:**949-59.

28. **Ryan, K. R., and L. Shapiro.** 2003. Temporal and spatial regulation in prokaryotic cell cycle progression and development. Annu Rev Biochem.

29. **Sackett, M. J., A. J. Kelly, and Y. V. Brun.** 1998. Ordered expression of ftsQA and ftsZ during the *Caulobacter crescentus* cell cycle. Mol Microbiol **28:**421-34.

30. **Santini, C. L., A. Bernadac, M. Zhang, A. Chanal, B. Ize, C. Blanco, and L. F. Wu.** 2001. Translocation of jellyfish green fluorescent protein via the Tat system of *Escherichia coli* and change of its periplasmic localization in response to osmotic up-shock. J Biol Chem **276:**8159-64.

31. **Schierle, C. F., M. Berkmen, D. Huber, C. Kumamoto, D. Boyd, and J. Beckwith.** 2003. The DsbA signal sequence directs efficient, cotranslational export of passenger proteins to the *Escherichia coli* periplasm via the signal recognition particle pathway. J Bacteriol **185:**5706-13.

32. **Shapiro, L., H. H. McAdams, and R. Losick.** 2002. Generating and exploiting polarity in bacteria. Science **298:**1942-6.

33. **Skerker, J. M., and L. Shapiro.** 2000. Identification and cell cycle control of a novel pilus system in *Caulobacter crescentus*. Embo J **19:**3223-34.

34. **Thomas, J. D., R. A. Daniel, J. Errington, and C. Robinson.** 2001. Export of active green fluorescent protein to the periplasm by the twin-arginine translocase (Tat) pathway in *Escherichia coli*. Mol Microbiol **39:**47-53.

35. **Weiss, D. S.** 2004. Bacterial cell division and the septal ring. Mol Microbiol **54:**588-97.

FIGURE LEGENDS

Figure 1. Schematic of *Caulobacter crescentus* cell cycle. The motile swarmer cell has a polar flagellum (wavy line) and several pili (straight lines), and does not replicate its DNA (nonreplicating DNA represented as a ring). During differentiation into a stalked cell, the flagellum is shed, the pili are retracted, a stalk is built at the same pole, and DNA replication initiates (theta structure). The stalked cell becomes a predivisional cell when it begins to constrict. Cell division yields a swarmer cell and a stalked cell.

Figure 2. CryoEM images of dividing Caulobacter cells. (A) Mid-cell slice of a tomogram of a predivisional cell showing rounded invagination forming at the division site. The inner (IM) and outer (OM) membranes are clearly visible surrounded by the fainter image of the S-layer (S). (B) Slice of a tomogram of a late-predivisional cell showing widening of the inner membrane-outer membrane spacing in the region of the constriction. The cytoplasm of the two nascent daughter cells is connected by a small tubular region. (C) Transmission EM (TEM) image of a cell after fission of the inner membrane and additional constriction of the outer membrane. The continuity of the periplasmic space surrounding the newly separated cytoplasmic compartments is evident. (D) TEM image of cell nearing fission of the outer membrane and cell separation. Restricted periplasmic diffusion may still be possible at this stage. (E) Divided cells. No division "scar" is visible at the poles of these cells. Note that we are assuming here that these two cells in close polar proximity are newly divided sibling cells, but we can not be absolutely sure that they are not two older cells caught in close proximity at the instant of freezing. (F) Drawing illustrating the minimum observed constrictions and radii of curvature of the inner (left) and outer (right) membranes.

Figure 3. (A) 3D rendering of a dividing cell just before inner membrane fission, constructed from the tomographic image data of the cell shown in Fig. 2B. The cytoplasm is shown in green, the inner membrane in yellow, and the outer membrane in orange. The 60 nm diameter channel connecting the cytoplasm of the nascent daughter cells is clearly visible. The spots within the cytoplasm are localized sites of high absorption that may be ribosomes. (B) Schematic in consistent scale showing stages of cell division corresponding to Figures 2A-E. Red: periplasm; Blue: cytoplasm. (C) Schematic of the progression of Escherichia coli cell division. (from Fig. 32 of Burdett and Murray, 1974.) (6) OM: outer membrane; ML: murein layer; IM: inner membrane.

Figure 4. (A) ssTorA-tdimer2 is in the periplasmic fraction of *Caulobacter* cells. LS4032 cells were separated into periplasmic (P) and spheroplast (SP) fractions as described in Materials and Methods. The total protein (T) is also shown. These fractions were probed with an anti-GFP antibody (top panel), and with an anti-tdimer2 antibody (bottom panel). The tdimer2 protein is two copies of the dimeric red fluorescent protein dimer2 (8)fused with a polypeptide linker. There is a band in the periplasmic fraction the size of the dimer2 protein, indicating that the ssTorA-tdimer2 protein is exported to the periplasm of *Caulobacter* cells and then cleaved into two parts. LS2677 is a control stain containing no fluorescent proteins. * is a non-specific band. (B) PilA-EGFP and CC2909-GFP are in the membrane fraction of *Caulobacter* cells. Cells containing pilA-EGFP (LS4026), and CC2909 (LS4029) were separated into the membrane (M) and soluble (S) fractions as described in Materials and Methods. The total protein (T) is also shown. These fractions were probed with an anti-GFP antibody (top panel), and with an anti-tdimer2 antibody (bottom panel). In strain LS4026, PilA-GFP is visible in the membrane fraction. A weaker and slightly smaller band (GFP*), presumably a breakdown product of PilA-GFP, is seen in the cytoplasmic fraction. Numbers on the left of each blot show the approximate molecular mass in kDa.

Figure 5. Compartmentalization of the periplasm. Four representative FLIP experiments using strain LS4032, containing cytoplasmic EGFP and periplasmic ssTorA-tdimer2. Images are false colored; green represents the fluorescence signal from EGFP, and red represents the florescence signal from ssTorA-tdimer2. (A) A LS4032 cell before (left panels) and 2 seconds after (second-from left panels) photobleaching. The cell-wide loss of fluorescence in both channels indicates that neither the cytoplasm nor the periplasm is compartmentalized. (B) The same experiment performed on another cell. The right panel shows an image of the cell taken 10 min after photobleaching. In this case, retention of fluorescence in both channels in the portion of the cell distal to the focused laser beam shows that both the membrane and the cytoplasm of this cell are compartmentalized. (C) In this cell, the cytoplasm is compartmentalized, but the periplasm is not, based on the picture taken 10 min after bleaching. (D) The cytoplasm of this cell is not compartmentalized. The periplasm appears to be compartmentalized in the image taken 20 s after bleaching. However, the image taken 10 min after bleaching shows that ssTorA-tdimer2 has diffused from the distal portion of the cell into the proximal portion, indicating that the periplasm is not fully compartmentalized. White circles: focused laser used for bleaching. The diameter of the circles is 0.4 μm: the full width half maximum size of the laser beam.

Figure 6. FLIP experiments on strains LS4026, containing PilA-EGFP (in the inner membrane) and cytoplasmic tdimer2, and LS4029, containing CC2909-EGFP (in the inner membrane) and cytoplasmic tdimer2. Images are false colored; green represents the fluorescence signal from CC2909-EGFP or PilA-EGFP. (A) shows a fluorescence image of a LS4029 cell before (left panels) and 2 seconds after (second-from left panels) photobleaching. The cell-wide loss of fluorescence indicates that CC2909-EGFP can diffuse past the constriction site. (B) The same experiment performed on a LS4026 cell. The cell-wide loss of fluorescence indicates that PilA-EGFP can diffuse past the constriction site. (C) The same experiment performed on another LS4029 cell. The membrane appears to be compartmentalized in the image taken 20 s after bleaching. However, the image taken 10 min after bleaching shows that CC2909-EGFP has diffused from the distal portion of the cell into the proximal portion. The diameter of the circles is 0.4 μm: the full width half maximum size of the laser beam.

Figure 1

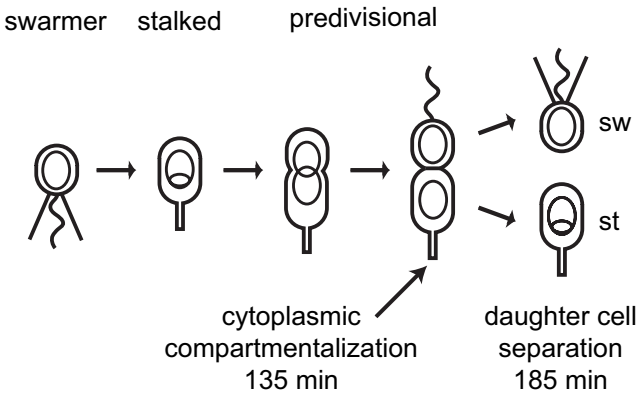
swarmer
stalked
predivisional
sw
st
cytoplasmic
compartmentalization
135 min
daughter cell
separation
185 min

Figure 2

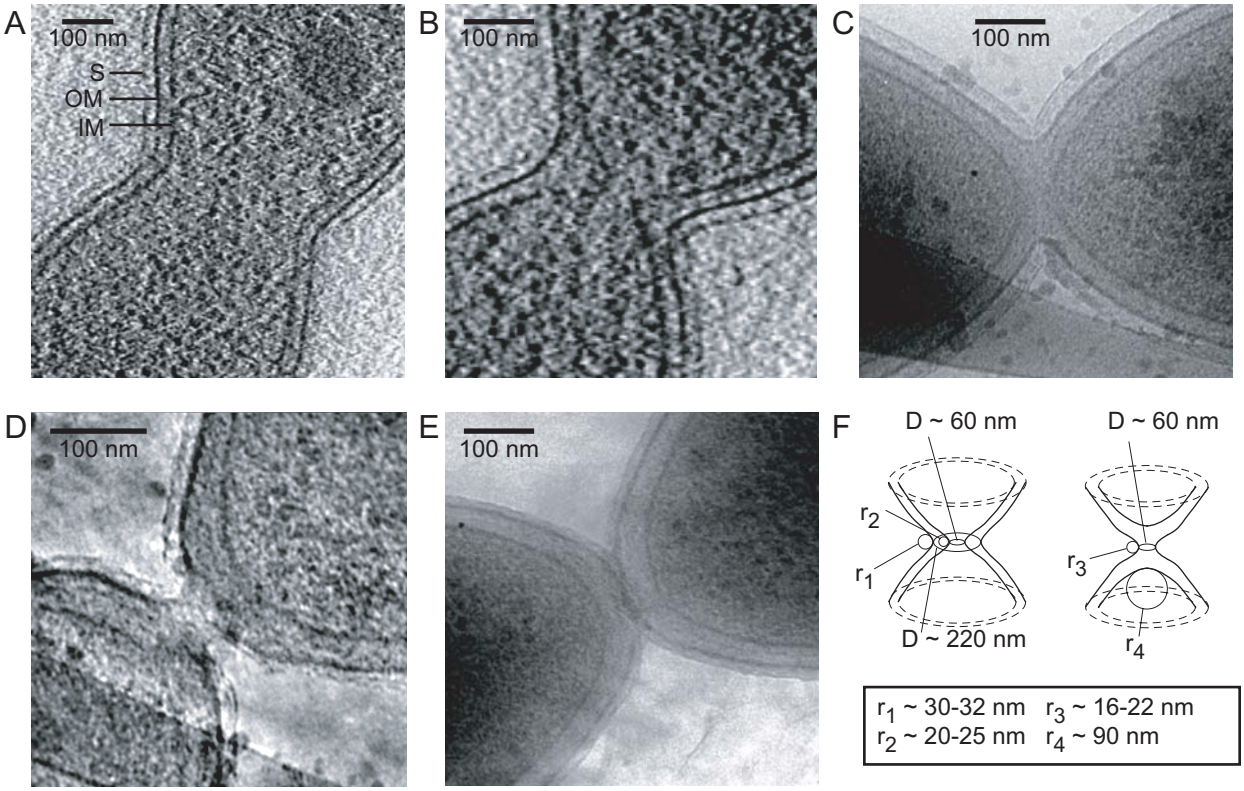
A
100 nm
S
OM
IM
B
100 nm
C
100 nm
D
100 nm
E
100 nm
F
D ~ 60 nm
D ~ 60 nm
r2
r1
D ~ 220 nm
r3
r4
r1 ~ 30-32 nm
r3 ~ 16-22 nm
r2 ~ 20-25 nm
r4 ~ 90 nm

Figure 3

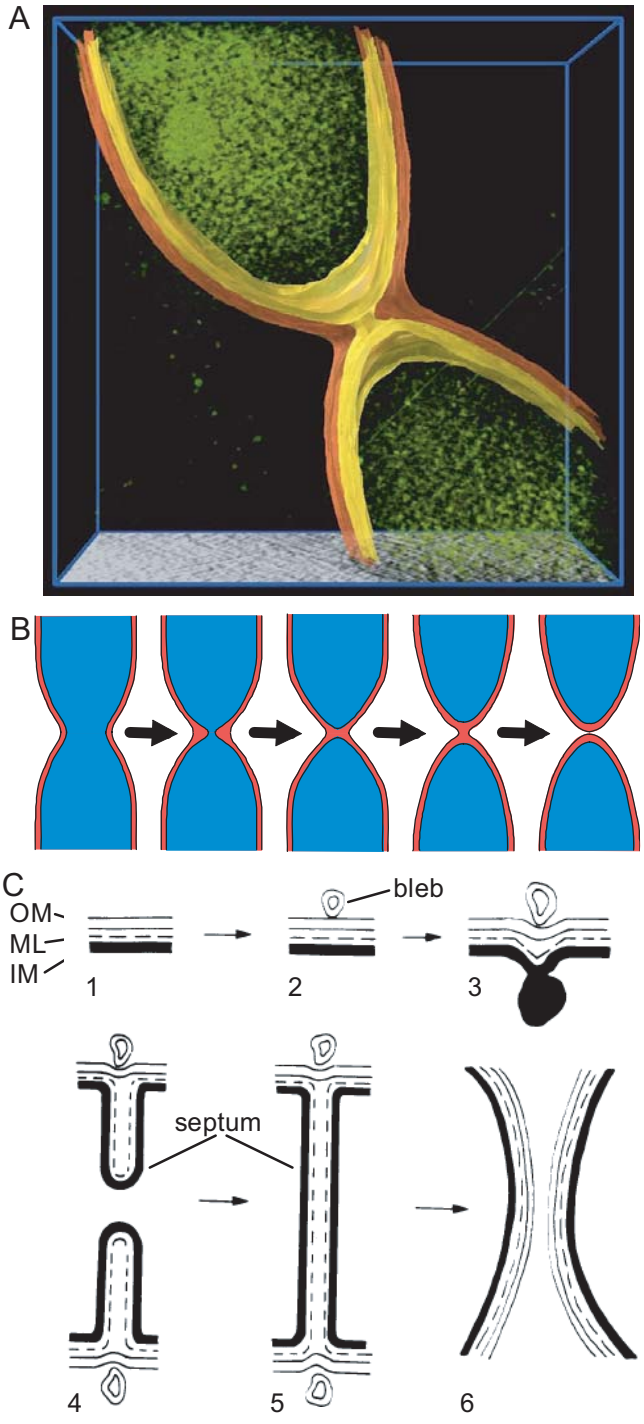

Figure 4

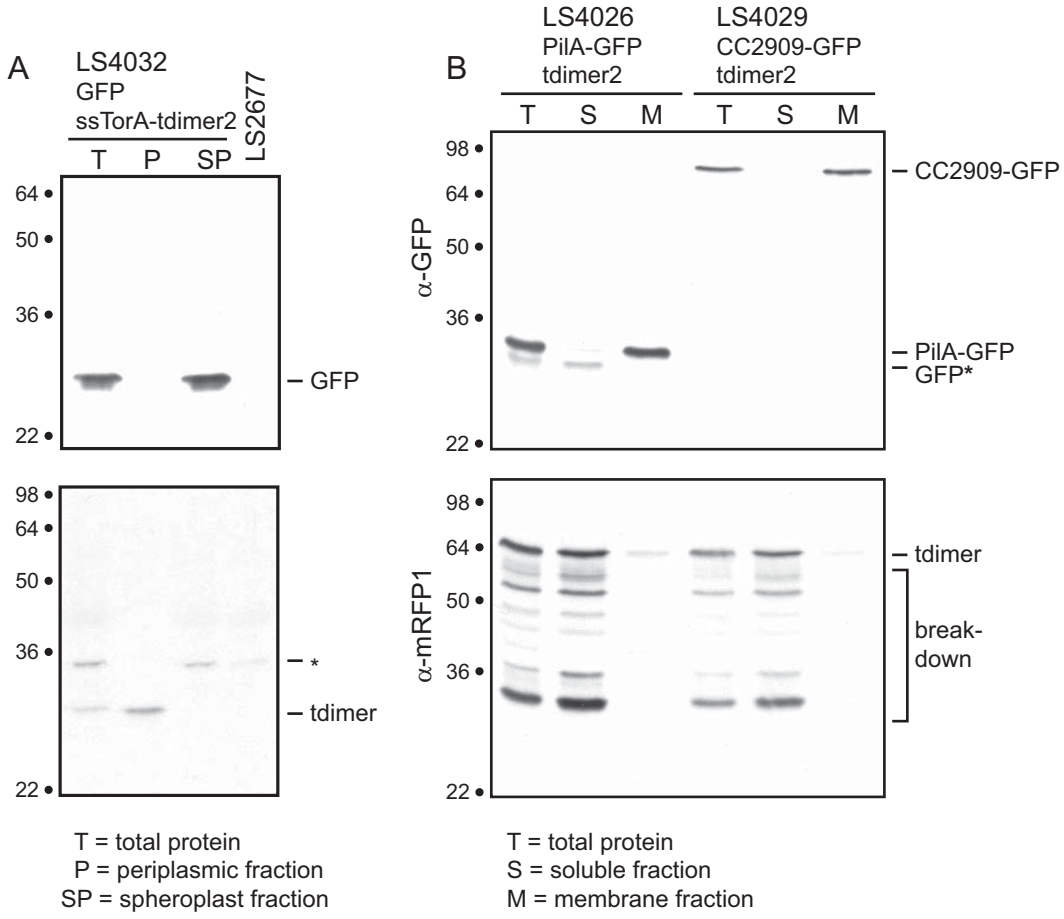
A
LS4032
GFP
ssTorA-tdimer2
LS2677
T
P
SP
64
50
36
22
GFP
98
64
50
36
22
*
tdimer
T = total protein
P = periplasmic fraction
SP = spheroplast fraction
B
LS4026
PilA-GFP
tdimer2
LS4029
CC2909-GFP
tdimer2
T
S
M
T
S
M
98
64
50
36
22
α-GFP
CC2909-GFP
PilA-GFP
GFP*
α-mRFP1
tdimer
break-
down
T = total protein
S = soluble fraction
M = membrane fraction

Figure 5

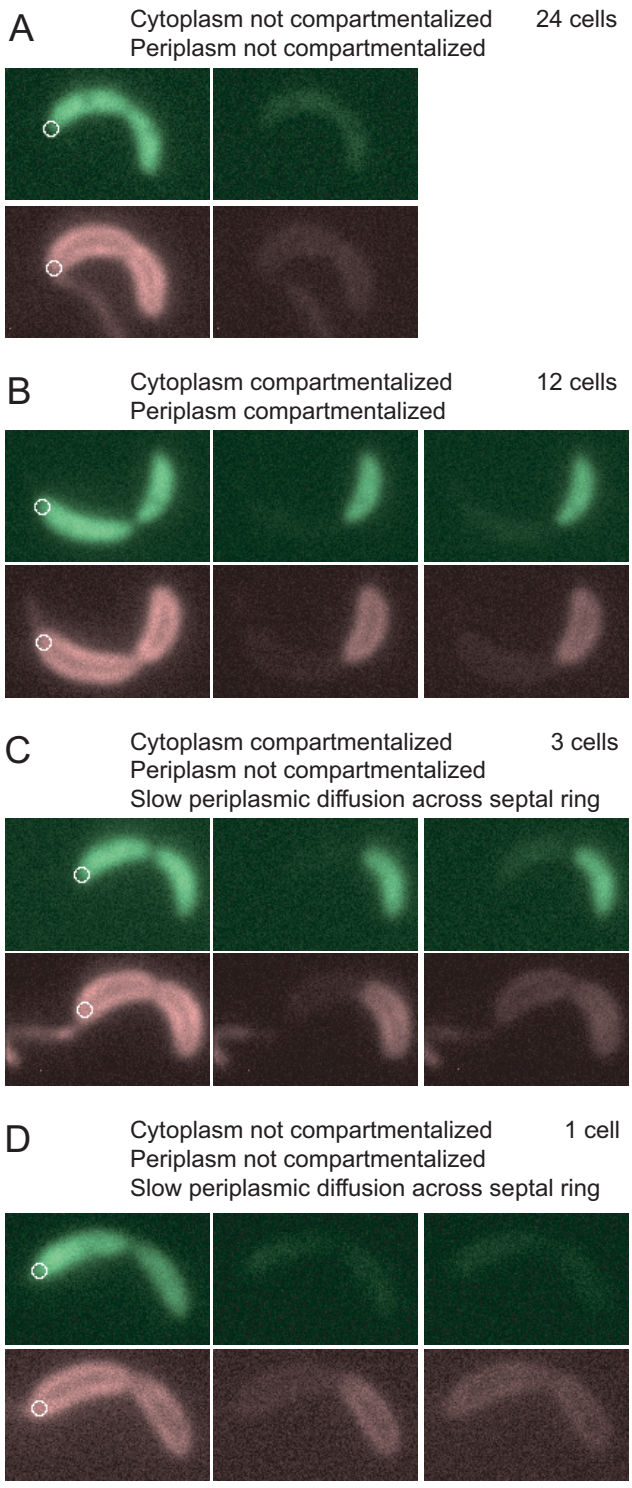
A
Cytoplasm not compartmentalized
Periplasm not compartmentalized
24 cells
B
Cytoplasm compartmentalized
Periplasm compartmentalized
12 cells
C
Cytoplasm compartmentalized
Periplasm not compartmentalized
Slow periplasmic diffusion across septal ring
3 cells
D
Cytoplasm not compartmentalized
Periplasm not compartmentalized
Slow periplasmic diffusion across septal ring
1 cell
Before bleaching
2 s after bleaching
10 min after bleaching

Figure 6

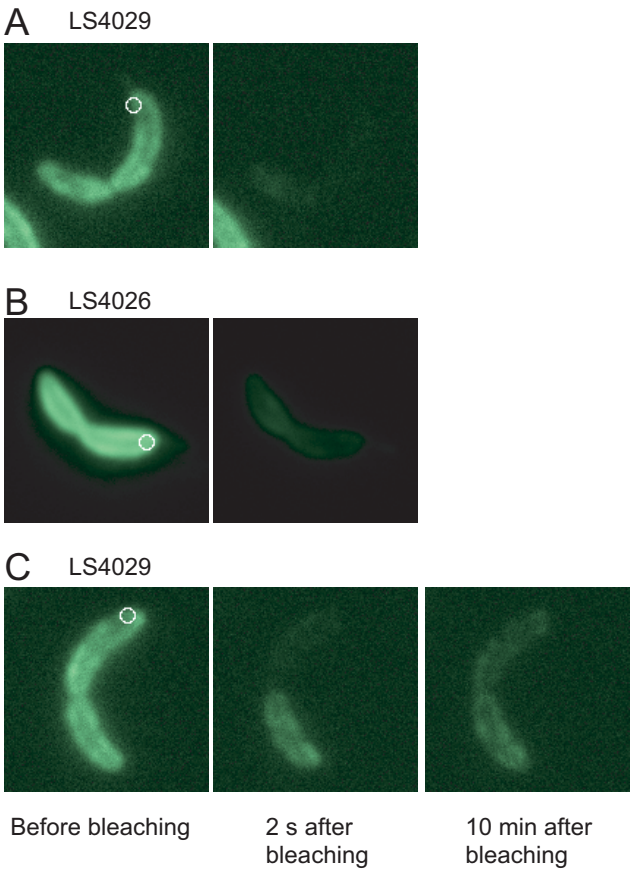
A
LS4029
B
LS4026
C
LS4029
Before bleaching
2 s after bleaching
10 min after bleaching